Challenges and implications of predicting the spatiotemporal distribution of dengue fever outbreak in Chinese Taiwan using remote sensing data and deep learning

Sumiko Anno, Hirakawa Tsubasa, Satoru Sugita, Shinya Yasumoto, Ming-An Lee, Yoshinobu Sasaki & Kei Oyoshi

Challenges and implications of predicting the spatiotemporal distribution of dengue fever outbreak in Chinese Taiwan using remote sensing data and deep learning

Sumiko Anno [a], Hirakawa Tsubasa [b], Satoru Sugita [b], Shinya Yasumoto [b], Ming-An Lee [c], Yoshinobu Sasaki [d] and Kei Oyoshi [d]

[a]Graduate School of Global Environmental Studies, Sophia University, Tokyo, Japan; [b]Chubu Institute for Advanced Studies, Chubu University, Aichi, Japan; [c]Centre of Excellence for Ocean Engineering and Department of Environmental Biology and Fisheries Science, National Taiwan Ocean University, Keelung, China; [d]Earth Observation Research Center, Japan Aerospace Exploration Agency, Ibaraki, Japan

ABSTRACT

Ongoing climate change has accelerated the outbreak and expansion of climate-sensitive infectious diseases such as dengue fever. Dengue fever will remain a threat until safe and effective vaccines and antiviral drugs have been developed, distributed, and administered on a global scale. By predicting the spatiotemporal distribution of dengue fever outbreaks, we can effectively implement dengue fever prevention and control. Our study aims to predict the spatiotemporal distribution of dengue fever outbreaks in Chinese Taiwan using a U-Net based encoder – decoder model with daily datasets of sea-surface temperature, rainfall, and shortwave radiation from Remote Sensing (RS) instruments and dengue fever case notification data. Although the prediction accuracy of the proposed model was low and the overlapping areas between the ground truth and pixelwise prediction were few, some of the pixels were located nearby the ground truth, suggesting that the application of RS data and deep learning may help to predict the spatiotemporal distribution of dengue fever outbreaks. With further improvements, the deep learning model might effectively learn a small amount of training data for a specific task.

1. Introduction

Ongoing climate change has accelerated the outbreak and expansion of climate-sensitive infectious diseases (Hoberg and Brooks 2015), especially mosquito-borne viral diseases such as dengue fever (Xu et al. 2017). Dengue fever is a notable climate-sensitive vector-borne viral disease that places 3.9 billion people at risk globally (World Health Organization 2020). The number of dengue fever patients has increased in Chinese Taiwan in recent years. In 2015, Chinese Taiwan recorded its largest dengue fever outbreak (43,774 cases) since case records began in 1998 (Taiwan 2016). Early forecasts of current dengue fever outbreak can assist the prevention and control of dengue fever (Buczak et al. 2014) until a specific antiviral therapy or a licensed vaccine becomes available (Vasilakis et al. 2011; Bekoe et al. 2017).

2. Related work

In previous studies, dengue fever outbreaks were predicted by spatial statistical methods (Banu et al. 2015; Chuang, Chaves, and Chen 2017) or machine learning with climatic variables (Guo et al. 2017; Carvajal et al. 2018). Banu et al. (2015) developed a predictive model for dengue fever incidence in Bangladesh which employs the El Niño Southern Oscillation (ENSO) and Indian Ocean Dipole indices. They suggested that the model fitness could be improved by employing more sophisticated models incorporating other factors to capture the nonlinear trends (Banu et al. 2015). Chuang, Chaves, and Chen (2017) developed a distributed lag nonlinear model that predicts dengue fever incidence in southern Taiwan, China using local climate variables, but admitted that more complicated mathematical/statistical models with various parameters are required for simulating a complex phenomenon. Combining machine learning with internet search queries and meteorological data, Guo et al. (2017) developed a support vector regression model for predicting dengue fever incidences at the province level. They reported that the model assisted the precise tracking of dengue fever dynamics. Carvajal et al. (2018) revealed that both the random forest and gradient boosting machine learning methods outperformed the conventional statistical modeling techniques in predicting the temporal pattern of dengue fever incidence in metropolitan Manila. They found that random forest with delayed meteorological effects best predicted the temporal pattern of dengue fever (Carvajal et al. 2018).

The above models cannot predict the spatiotemporal distributions with sufficient accuracy for implementing effective dengue fever control and prevention. Such models must also reflect the transmission dynamics of dengue fever and consider the multiple variables of disease spread. In recent years, deep learning models have proven especially effective in spatiotemporal predictions such as climate forecasts (Shi et al. 2015) and traffic prediction (Ma et al. 2017). However, the spatiotemporal spread of infectious diseases has not yet been predicted by deep learning models because the disease dynamics are related in complex ways to multiple climatic factors. The multitude of factors complicating spatiotemporal dependence makes capturing true spatiotemporal dynamic behavior more difficult (Tan, Liu, and Liu 2021). Satellite Remote Sensing (RS) data can be used to not only capture the true spatiotemporal dynamic behavior of dengue fever outbreaks, but also to provide data on multiple climatic factors influencing dengue fever outbreaks across the spatiotemporal continuum. RS data on sea surface temperature, rainfall, and shortwave radiation as temperature, all of which are thought to influence dengue fever outbreaks, are available daily and over a large area. Deep learning and RS data could be used to predict spatiotemporal distribution of dengue fever outbreaks with high accuracy. Thereafter, we aimed to integrate spatiotemporal data on climatic factors obtained from satellite RS with data on dengue fever cases. The combined data is fed into a deep learning model that forecasts the spatiotemporal distribution of dengue fever outbreaks in Chinese Taiwan.

3. Methodology

3.1. Study area

Our study area was Chinese Taiwan, which consists of 368 townships. The climate is subtropical in the north and tropical in the south. Dengue fever outbreaks mainly occur in southwestern Chinese Taiwan, with 90% of all dengue fever cases reported in Kaohsiung and Tainan Cities. Transmission usually starts in June and peaks in October and November, indicating strong seasonality (Chuang, Chaves, and Chen 2017).

3.2. Deep learning experiment

3.2.1. Data collection and preprocessing

The case registry of dengue fever, announced as a Notified Infectious Disease (NID), has been collected continuously and systematically by the NID Notification Surveillance System since 1998 (https://data.gov.tw/dataset/21025). The Chinese Taiwan Centre for Disease Control (CDC) computerized database records the daily notification of each dengue fever case, including the date of disease onset, gender, age group, patient's place of residence (township or village), and the longitude and latitude indicating the central coordinate of each patient's residence (township or village). These data were used as the experimental dataset.

The experiment additionally used three climatic data confirmed to be strongly associated with dengue fever outbreaks in previous studies (Banu et al. 2015; Chuang, Chaves, and Chen 2017; Guo et al. 2017; Carvajal et al. 2018): the daily RS data on sea-surface temperature, the rainfall data, and shortwave radiation data.

The sea-surface temperatures at a spatial resolution of 4 km from the Advanced Very High Resolution Radiometer Pathfinder version 5.3 were obtained from the Environmental Research Division's Data Access Program (ERDDAP) website (https://coastwatch.pfeg.noaa.gov/erddap) (Simons 2016) of the U. S. National Oceanic and Atmospheric Administration.

The rainfall data, obtained from Japan Aerospace Exploration Agency (JAXA) (https://sharaku.eorc.jaxa.jp/GSMaP/index.htm), were generated using the Global Satellite Mapping of Precipitation (GSMaP) product which is made up of a number of satellites equipped with optical sensors, microwave radiometers, and radar (Kubota et al. 2007). The GSMaP products are integrated hourly on a 0.1°-sized grid. We used the 24-h averaged rainfall derived from the GSMaP hourly product, which has the same spatial resolution as the hourly product.

The shortwave radiation data were generated using the data collected by the Moderate Resolution Imaging Spectroradiometer (MODIS) onboard the Terra and Aqua satellites operated by National Aeronautics and Space Administration (NASA). The daily shortwave radiation data employed in this study were obtained from the JAXA Satellite Monitoring for Environmental Study (JASMES, https://www.eorc.jaxa.jp/JASMES/index.html) (Frouin and Murakami 2007; Saigusa et al. 2010). The data are obtained at a spatial grid resolution of 0.05°. Daily shortwave radiation data measured by Terra (at 10:30 local time) or Aqua (at 13:30 local time) are available at JASMES. We constructed a map by averaging over the Terra and Aqua satellite data to obtain the daily product.

Figure 1 presents the data collection and preprocessing steps of the present experiment. The original RS data and dengue fever case notification data were obtained from the aforementioned websites via Python-based file download scripts that automatically download web content. The RS data were stored locally and preprocessed through the following steps: (1) generate a number of 384 × 512-pixel images corresponding to the number of days from 2002/4/16 to

1. Collect RS and dengue fever data from the web sites using Python-based file download scripts.
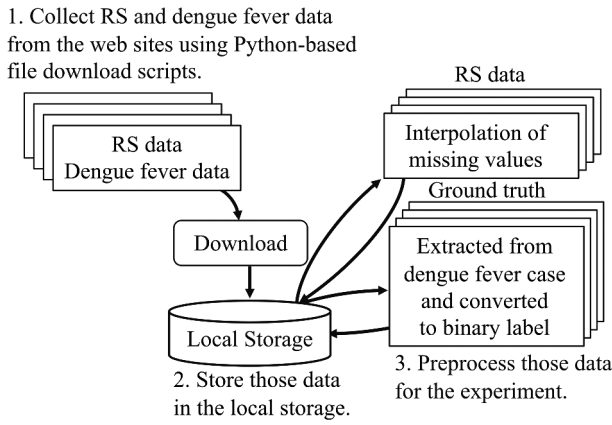

Figure 1. Data collection and preprocessing steps of the proposed method.

2020/9/30, (2) interpolate the missing values based on distance measures between pairs, (3) normalize the data to the range (0, 1), and (4) integrate the daily data from 2002/4/16 to 2020/9/30 into two-weekly intervals. The last step (compiling the data into fortnightly intervals) was necessary because very few cases of dengue fever were recorded per day throughout the experimental period. The RS data on sea-surface temperature, rainfall, and shortwave radiation were converted into Numpy array format and input to the model. The size of converted array is 384×512, where the size of each grid corresponds to approximately $1 \, km^2$. The ground truth label extracted from the dengue fever case notification data was converted to a binary label of size 384×512 for fitting into the converted RS data, where each pixel is labeled (one-hot encoded) as 1 if the dengue fever outbreak is present at that pixel and 0 otherwise. The result is the output of the model.

3.2.2. Experimental study

We employed a U-Net based encoder – decoder model, which possesses a two-part architecture: a contracting path and an expanding path that enables precise localization (Ronneberger, Fischer, and Brox 2015). The U-Net model works with remarkably few training images and yields more precise semantic segmentation

when provided with the location information (Bai, Mas, and Koshimura 2018). For precise image localization, the algorithm assigns the output class label to specific pixels. The architecture of the network used in our study is shown in Figure 2. The contracting path repeatedly applies two 3×3 convolutions (unpadded convolutions), each followed by a rectified linear unit (ReLU), and a 2×2 max pooling operation with a stride of 2 for downsampling. At each downsampling step, the number of feature channels starts from 3 and doubles until it reaches 512. The expanding path recovers the original dimensions of the input images by upsampling the feature map. This path performs a 2×2 convolution (up-convolution) that halves the number of feature channels, a concatenation with the correspondingly cropped feature map from the contracting path, and two 3×3 convolutions. Each process of the expanding path except the first is followed by a ReLU. In the final layer of the expanding path, a 1×1 convolution maps each 2-component feature vector to the desired number of classes (Ronneberger, Fischer, and Brox 2015).

The experimental inputs were the following five datasets composed of different data: 1) sea-surface temperature, rainfall, and shortwave radiation, 2) sea-surface temperature, 3) rainfall, 4) shortwave radiation, and 5) rainfall and shortwave radiation. Each input was a data-integrated $384 \times 512 \times 3$ channel image. The output was a $384 \times 512 \times 2$ image in which the first and second channels represented the probability of the absence and presence of dengue fever outbreak, respectively. The network was trained on the input and output images using the PyTorch implementation. Specifically, we inputted the preprocessed RS images to the model and trained the network to predict the target output. Among the datasets created from 2002/4/16 to 2020/9/30, we selected the 2002/4/16 to 2017/12/31 data for training, the 2018/1/1 to 2018/12/31 data for validation, and the 2019/1/1 to 2020/9/22 data for testing. Each dataset's model was trained for 2000 epochs, with eight batches per epoch. The loss function was minimized during training using a Stochastic Gradient Descent (SGD) optimizer with a learning rate of 0.01 and a momentum of 0.9.
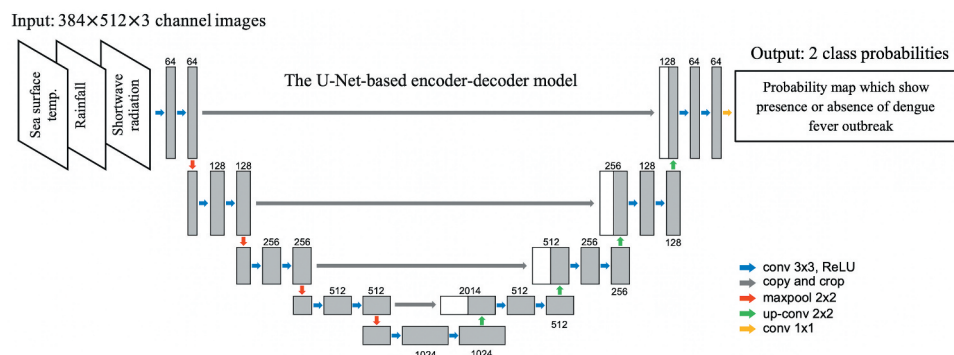

Figure 2. Training of the U-Net based encoder – decoder model.

To assess the model performance, the training model was applied to the validation dataset. In the validation process, the hyperparameters (learning rate and batch size) were optimized by tuning and the patch size was optimized as described above. The performance of the training model was then evaluated on the testing dataset.

3.2.3. Assessment of model performance

The experimental results were evaluated by various quantitative metrics: overall accuracy, mean accuracy, mean Intersection over Union (mean IoU), frequency weighted accuracy/frequency weighted intersection over union (FWA/FWIoU), and the Dice Index (DI) coefficient. The overall accuracy is an agreement measure that indicates the percentage of correctly classified pixels (Brovelli et al. 2015). The mean accuracy, which refers to the percentage of correctly classified pixels in each category, is calculated by averaging the overall accuracy over all classes (Ma et al. 2019). In each class, the IoU is calculated as the ratio of correctly classified pixels to the total number of ground truth and predicted pixels in that class. The mean IoU of each class is weighted by the number of pixels in that class (Abdelhafiz et al. 2020). The FWA/FWIoU is an extension of MIoU in which each class is weighted according to its frequency (Ma et al. 2019). The DI measures the similarity between the ground truth and prediction at each pixel. DI scores range from 0 to 1 (0 to 100%), where 0 and 1 signify no overlap and perfect overlap, respectively, between the ground truth and prediction at each pixel (Abdelhafiz et al. 2020).

4. Results

The evaluation results (overall accuracy, mean accuracy, mean IoU, FWA/FWIoU, and DI) of the five models trained on the five testing datasets with various data combinations are shown in Table 1. When evaluating the model performances, all predictions were compared with the pixel-level ground truth values. The overall accuracy scores of all models approximated 0.999. The mean accuracy, mean IoU, FWA/FWIoU, and DI scores of all models were around 0.501–0.509, 0.500–0.504, 0.997–0.999, and 0.001–0.018, respectively. The low DI coefficients indicated that the models poorly localized the outbreak region, resulting in lowered prediction accuracy. Although the mean accuracies, mean IoUs, and DI coefficients were low, the overall accuracies and FWA/FWIoU ratios were reasonable. Note that in binary (two-class) prediction, high pixel accuracy does not always imply superior prediction ability because the classes may be imbalanced. The performances of the five models were similar but the models using the combined data (sea-surface temperature + rainfall + shortwave radiation and rainfall + shortwave radiation) slightly outperformed the other models. Tables 2 and 3 show, in addition to the accuracy for the testing dataset, the accuracy for the training and validation datasets.

Figure 3 presents some selected visual results after testing on the testing datasets. The left image is the corresponding binary ground truth image and the center and right images are the binarized images output by the models on the testing datasets. Although the regions of dengue fever outbreak (white pixels in

Table 1. Quantitative performance measures of the model on testing dataset.

Testing dataset	Overall Accuracy	Mean Accuracy	Mean Intersection over Union	Frequency Weighted Accuracy	Dice index coefficient
SST+R+SWR[a]	0.999,845	0.509,462	0.504,506	0.997,7	0.018,169
SST	0.999,557	0.502,009	0.500,152	0.999,481	0.001,494
R	0.999,875	0.501,437	0.500,82	0.999,799	0.003,524
SWR	0.999,903	0.503,644	0.502,796	0.999,828	0.011,312
R+SWR	0.999,872	0.507,283	0.504,232	0.999,797	0.017,036

[a]SST: Sea-surface temperature; R = rainfall; SWR= shortwave radiation.

Table 2. Quantitative performance measures of the model on training dataset.

Training dataset	Overall Accuracy	Mean Accuracy	Mean Intersection over Union	Frequency Weighted Accuracy	Dice index coefficient
SST+R+SWR[a]	0.999,739	0.604,461	0.573,842	0.999,553	0.257,756
SST	0.999,423	0.508,670	0.503,024	0.999,208	0.013,162
R	0.999,513	0.504,889	0.501,988	0.999,297	0.008,888
SWR	0.999,812	0.620,313	0.608,576	0.999,642	0.357,073
R+SWR	0.999,787	0.558,353	0.553,023	0.999,593	0.192,105

[a]SST: Sea-surface temperature; R = rainfall; SWR= shortwave radiation.

Table 3. Quantitative performance measures of the model on validation dataset.

Validation dataset	Overall Accuracy	Mean Accuracy	Mean Intersection over Union	Frequency Weighted Accuracy	Dice index coefficient
SST+R+SWR[a]	0.999,796	0.508,454	0.503,704	0.999,705	0.015,109
SST	0.999,543	0.504,072	0.500,627	0.999,451	0.003,414
R	0.999,812	0.501,016	0.500,424	0.999,720	0.002,073
SWR	0.999,864	0.504,233	0.502,802	0.999,773	0.011,412
R+SWR	0.999,861	0.504,232	0.502,736	0.999,770	0.011,158

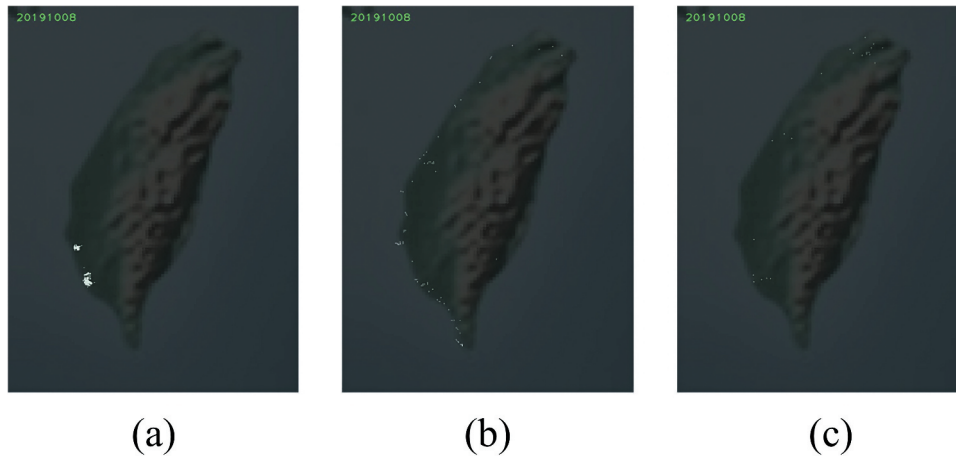[a]SST: Sea-surface temperature; R = rainfall; SWR= shortwave radiation.

(a) (b) (c)

Figure 3. Experimental results showing: (a) the corresponding binary ground truth image dated 2019/10/08, (b) the predicted image of the model on the testing dataset combining the sea-surface temperature, rainfall, and shortwave radiation dated 2019/10/08, and (c) the predicted image of the model on the testing dataset combining the rainfall and shortwave radiation dated 2019/10/08 (white pixels: predicted dengue fever outbreak; black pixels: no predicted dengue fever outbreak). Video clips 1A-1F. Experimental results. The video clip shows: (a) the corresponding binary ground truth movie from 2019/1/1 to 2020/9/22, (b) the predicted movie on the testing datasets based on combinations of sea-surface temperature, rainfall, and shortwave radiation from 2019/1/1 to 2020/9/22, (c) the predicted movie on the testing datasets based on sea-surface temperature from 2019/1/1 to 2020/9/22, (d) the predicted movie on the testing datasets based on rainfall from 2019/1/1 to 2020/9/22, (e) the predicted movie on the testing datasets based on shortwave radiation from 2019/1/1 to 2020/9/22, (f) the predicted movie on the testing datasets based on combinations of rainfall and shortwave radiation from 2019/1/1 to 2020/9/22.

Figure 3) predicted by the model appear in southwestern Taiwan, China, where dengue fever is endemic, few of the white pixels overlap with those of the ground truth, reflecting the low evaluation metrics.

Video clips 1A–1F present movies of the binary ground truth (clip 1A) and all model evaluations on the testing datasets (clips 1B–1F). On the testing datasets of sea-surface temperature, rainfall, and shortwave radiation (clips 1C, 1D, and 1E, respectively), the white pixels are expressed in southwestern Taiwan from June to December, predicting a seasonal distribution around the dengue fever endemic area. On the testing datasets of combined sea-surface temperature, rainfall, and shortwave radiation (clip 1B) and combined rainfall and shortwave radiation (clip 1F), the white pixels are expressed throughout the year in western Taiwan, China, showing no seasonality. Overall, few overlapping areas appear between the ground truth and the prediction results.

5. Discussion

The U-Net based encoder – decoder model showed low performance for pixelwise prediction on the testing datasets. These results can be attributed to the learning of binary predictions from imbalanced data, which are characterized by large bias in distributions of the target/objective variables. When regression models are trained on highly skewed (imbalanced) datasets, their predictive capability is notably weak (Yu et al. 2017; Gurita and Mocanu 2021). In the present study, the number of dengue fever cases was almost zero except during the 2015 outbreaks. Moreover, although the dengue fever cases were dominant in southwestern Taiwan, China, they occurred in different locations on each day. Such an imbalanced distribution of the target/objective variable values may have degraded the model performance for predicting the spatiotemporal distribution of dengue fever outbreaks.

The low performance results are also attributable to the small amount of training data for the specific task in satellite images. When few training data are available as features in satellite images, they cannot participate in the training of the network. During training, deep learning algorithms tend to lose the information of small objects, leading to poor performance for small local objects and consequent reduction in accuracy (Men et al. 2017; Yan et al. 2019). In a previous spatiotemporal hotspot analysis and machine learning study of dengue fever in Chinese Taiwan (Anno et al. 2019), sea-surface temperature was identified as a predominant influencer of dengue fever outbreaks. However, when the model was applied to the testing dataset of sea-surface temperature, it yielded the lowest DI coefficient because RS data on sea-surface temperatures were missing over land. Owing to both the limited number of training dataset in each fold and the many deficit values in the RS data, we considered that the network could not effectively learn the necessary features for the prediction task.

6. Conclusions

In this work, we applied the first deep learning model to the prediction of the spatiotemporal distribution of dengue fever cases using RS data. Previous studies predicted dengue fever outbreaks at the country-region level, but this study improves them to the location-specific level. The use of a location-specific model allows for more rapid and accurate intervention and control. Although most of the pixels predicted by the trained model did not overlap with the ground truth, some of the pixels were located nearby the ground truth, indicating that the spatiotemporal prediction of dengue fever outbreak is possible with RS data. This possibility is expected to be enhanced by a better deep learning model that can learn effectively with a small amount of training data, using high-resolution RS data from NASA Power, and developing a new resampling approach to overcome the data imbalance problem and model overfitting. Spatiotemporal visualizations generated by deep learning models can potentially guide the implementation of effective measures against the epidemic at the most likely times and locations for disease prevention and control.

Disclosure statement

No potential conflict of interest was reported by the author(s).

Funding

Notes on contributors

Sumiko Anno is a professor at the Graduate School of Global Environmental Studies, Sophia University. Her research interests include applications of remote sensing, geographic information systems, and machine/deep learning to public health.

Tsubasa Hirakawa is a lecturer at the Center for Mathematical Science and Artificial Intelligence, Chubu University. His research interests include computer vision, pattern recognition, and machine learning.

Satoru Sugita is an associate professor at International Digital Earth Applied Science Research Center, Chubu University. His research interests include digital earth, high-resolution remote sensing, and geographic information systems.

Shinya Yasumoto is an associate professor at Department of History and Geography, College of Humanities, Chubu University. His research interests include geographic information systems and digital earth.

Ming-An Lee is a distinguish professor at the doctor degree program in ocean science and environmental change, National Taiwan Ocean University. His research interests include satellite oceanography, fishery instruments, and descriptive fishery oceanography.

Yoshinobu Sasaki is a senior researcher at Earth Observation Research Center (EORC), Japan Aerospace Exploration Agency (JAXA). He has engaged in research and development of earth observation satellite data analysis, promotion of data utilization, and development of tools and systems.

Kei Oyoshi is a senior researcher at EORC, JAXA. His research interests include spatiotemporal image processing, and applications of remote sensing technology to agriculture, public health and environmental monitoring.

ORCID

Sumiko Anno ⓘ http://orcid.org/0000-0003-2962-6093
Hirakawa Tsubasa ⓘ http://orcid.org/0000-0003-3851-5221
Satoru Sugita ⓘ http://orcid.org/0000-0003-2965-1475
Shinya Yasumoto ⓘ http://orcid.org/0000-0002-4840-0420
Ming-An Lee ⓘ http://orcid.org/0000-0001-6970-7643
Yoshinobu Sasaki ⓘ http://orcid.org/0000-0002-3398-454X
Kei Oyoshi ⓘ http://orcid.org/0000-0001-9704-4998

Data availability statement

The source code and data supporting the findings of this study are available at the website https://github.com/thirakawa/dengue feverPredictionUNet.

References

Abdelhafiz, D., J. Bi, R. Ammar, C. Yang, and S. Nabavi. 2020. "Convolutional Neural Network for Automated Mass Segmentation in Mammography." *BMC Bioinformatics* 21 (S1): 192. doi:10.1186/s12859-020-3521-y.

Anno, S., T. Hara, H. Kai, M.A. Lee, Y. Chang, K. Oyoshi, Y. Mizukami, and T. Tadono. 2019. "Spatiotemporal Dengue Fever Hotspots Associated with Climatic Factors in Taiwan Including Outbreak Predictions Based on Machine-Learning." *Geospatial Health* 14 (2): 183–194. doi:10.4081/gh.2019.771.

Bai, Y., E. Mas, and S. Koshimura. 2018. "Towards Operational Satellite-Based Damage-Mapping Using U-Net Convolutional Network: A Case Study of 2011 Tohoku Earthquake-Tsunami." *Remote Sensing* 10 (10): 1626. doi:10.3390/rs10101626.

Banu, S., Y. Guo, W. Hu, P. Dale, J. S. Mackenzie, K. Mengersen, and S. Tong. 2015. "Impacts of El Niño Southern Oscillation and Indian Ocean Dipole on Dengue Incidence in Bangladesh." *Scientific Reports* 5 (1): 16105. doi:10.1038/srep16105.

Bekoe, C., T. Pansombut, P. Riyapan, S. Kakchapati, and A. Phon-On. 2017. "Modeling the Geographic Consequence and Pattern of Dengue Fever Transmission in Thailand." *Journal of Health Science Research* 17 (2): e00378.

Brovelli, M. A., M. E. Molinari, E. Hussein, J. Chen, and R. Li. 2015. "The First Comprehensive Accuracy Assessment of Globeland30 at a National Level: Methodology and Results." *Remote Sensing* 7 (4): 4191–4212. doi:10.3390/rs70404191.

Buczak, A. L., B. Baugher, S. M. Babin, L. C. Ramac-Thomas, E. Guven, Y. Elbert, P. T. Koshute, et al. 2014. "Prediction of High Incidence of Dengue fever in the Philippines." *PLoS Neglected Tropical Diseases* 8 (4): e2771. doi:10.1371/journal.pntd.0002771. PMID: 24722434; PMCID: PMC3983113.

Carvajal, T. M., K. M. Viacrusis, L. F. T. Hernandez, H. T. Ho, D. M. Amalin, and K. Watanabe. 2018. "Machine Learning Methods Reveal the Temporal Pattern of Dengue Fever Incidence Using Meteorological Factors on Metropolitan Manila, Philippines." *BMC Infectious Diseases* 18 (1): 183. doi:10.1186/s12879-018-3066-0.

Chuang, T. W., L. F. Chaves, and P. J. Chen. 2017. "Effects of Local and Regional Climatic Fluctuations on Dengue Fever Outbreaks in Southern Taiwan." *Plos One* 12 (6): e0178698. doi:10.1371/journal.pone.0178698.

Frouin, R., and H. Murakami. 2007. "Estimating Photosynthetically Avail Imager Data." *Journal of Oceanography* 63 (3): 493–503. doi:10.1007/s10872-007-0044-3.

Guo, P., T. Liu, Q. Zhang, L. Wang, J. Xiao, Q. Zhang, G. Luo, et al. 2017. "Developing a Dengue fever Forecast Model Using Machine Learning: A Case Study in China." *PLoS Neglected Tropical Diseases* 11 (10): e0005973. doi:10.1371/journal.pntd.0005973.

Gurita, A., and I. G. Mocanu. 2021. "Image Segmentation Using Encoder-Decoder with Deformable Convolutions." *Sensors* 21 (5): 1570. doi:10.3390/s21051570.

Hoberg, E. P., and D. R. Brooks. 2015. "Evolution in Action: Climate Change, Biodiversity Dynamics and Emerging Infectious Disease." *Philosophical Transactions of the Royal Society B: Biological Sciences* 370 (1665): 20130553. doi:10.1098/rstb.2013.0553.

Kubota, T., S. Shige, H. Hashizume, K. Aonashi, N. Takahashi, S. Seto, M. Hirose, et al. 2007. "Global Precipitation Map Using Satellite Borne Microwave Radiometers by the Gsmap Project: Production and Validation." *IEEE Transactions on Geoscience and Remote Sensing* 45 (7): 2259–2275. doi:10.1109/TGRS.2007.895337.

Ma, X., Z. Dai, Z. He, J. Ma, Y. Wang, and Y. Wang. 2017. "Learning Traffic as Images: A Deep Convolutional Neural Network for Large-Scale Transportation Network Speed Prediction." *Sensors* 17 (4): 818. doi:10.3390/s17040818.

Ma, X., X. Deng, L. Qi, Y. Jiang, H. Li, Y. Wang, and X. Xing. 2019. "Fully Convolutional Network for Rice Seedling and Weed Image Segmentation at the Seedling Stage in Paddy Fields." *Plos One* 14 (4): e0215676. doi:10.1371/journal.pone.0215676. PMID: 30998770; PMCID: PMC6472823.

Men, K., X. Chen, Y. Zhang, T. Zhang, J. Dai, J. Yi, and Y. Li. 2017. "Deep Deconvolutional Neural Network for Target Segmentation of Nasopharyngeal Cancer in Planning Computed Tomography Images." *Frontiers in Oncology* 7: 315. doi:10.3389/fonc.2017.00315.

Ronneberger, O., P. Fischer, and T. Brox. 2015. "U-Net: Convolutional Networks for Biomedical Image Segmentation." In *Medical Image Computing and Computer-Assisted Intervention–MICCAI 2015. MICCAI 2015. Lecture Notes in Computer Science*, 9351 Vols. edited by N. Navab, J. Hornegger, W. Wells, and A. Frangi, Cham: Springer. doi:10.1007/978-3-319-24574-4_28.

Saigusa, N., K. Ichii, H. Murakami, R. Hirata, J. Asanuma, H. Den, S. J. Han, et al. 2010. "Impact of Meteorological Anomalies in the 2003 Summer on Gross Primary Productivity in East Asia." *Biogeoscience* 7 (2): 641–655. doi:10.5194/bg-7-641-2010.

Shi, X., Z. Chen, H. Wang, D. -Y. Yeung, W. -K. Wong, and W. -C. Woo. 2015. "Convolutional LSTM Network: A Machine Learning Approach for Precipitation Nowcasting." Proceedings of the Twenty-Ninth Annual Conference on Neural Information Processing Systems (NIPS), Montreal, Canada, Curran Associates Inc.

Simons, R. A. 2016. ERDDAP. Monterey, CA: NOAA/NMFS/SWFSC/ERD. https://coastwatch.pfeg.noaa.gov/erddap

Taiwan, C.D.C. 2016. "Taiwan National Infectious Disease Statistics System." Taiwan Centers for Disease Control, Taiwan, China. http://www.cdc.gov.tw/rwd/english

Tan, Q., Y. Liu, and J. Liu. 2021. "Demystifying Deep Learning in Predictive Spatiotemporal Analytics: An Information-Theoretic Framework." IEEE Transactions on Neural Networks and Learning Systems, 32 (8): 3538–3552. doi:10.1109/TNNLS.2020.3015215.

Vasilakis, N., J. Cardosa, K. A. Hanley, E. C. Holmes, and S. C. Weaver. 2011. "Fever from the Forest: Prospects for the Continued Emergence of Sylvatic Dengue Fever Virus and Its Impact on Public Health." *Nature Reviews: Microbiology* 9 (7): 532–541. doi:10.1038/nrmicro2595.

World Health Organization. 2020. "Dengue Fever and Severe Dengue Fever." Accessed August 2020. https://www.who.int/news-room/fact-sheets/detail/Denguefever-and-severe-dengue

Xu, L., L. C. Stige, K. S. Chan, J. Zhou, J. Yang, S. Sang, M. Wang, et al. 2017. "Climate Variation Drives Dengue Fever Dynamics." *Proceedings of the National Academy of Sciences of the United States of America* 114 (1): 113–118. doi:10.1073/pnas.1618558114.

Yan, J., H. Wang, M. Yan, W. Diao, X. Sun, and H. Li. 2019. "Iou-Adaptive Deformable R-CNN: Make Full Use of Iou for Multi-Class Object Detection in Remote Sensing Imagery." *Remote Sensing* 11 (3): 286. doi:10.3390/rs11030286.

Yu, X., J. Liu, Z. Yang, X. Jia, Q. Ling, and S. Ye. 2017. "Learning from Imbalanced Data for Predicting the Number of Software Defects." IEEE 28th International Symposium on Software Reliability Engineering (ISSRE), 78–89. doi:10.1109/ISSRE.2017.18.